




Article

Effect of Sandstone Pore Morphology on Mechanics, Acoustic Emission, and Energy Evolution

Gang Liu ^{1,2}, Dongwei Wang ^{1,*}, Shengxuan Wang ¹, Yonglong Zan ¹, Qiqi Zhang ¹, Zhitao Yang ^{2,*}, Jiazhen Li ^{2,3} and Zhen Wei ⁴

¹ Heilongjiang Ground Pressure and Gas Control in Deep Mining Key Laboratory, Heilongjiang University of Science and Technology, Harbin 150022, China; liugang@usth.edu.cn (G.L.); w13140438798@163.com (S.W.); 17353693207@163.com (Y.Z.); zqq1162170954@163.com (Q.Z.)

² Baotailong New Material Co., Ltd., Postdoctoral Research Station, Beijing 100000, China; lijiazhen@usth.edu.cn

³ Postdoctoral Research Station of Safety Science and Engineering, Heilongjiang University of Science and Technology, Harbin 150022, China

⁴ School of Civil Engineering, Lanzhou Institute of Technology, Lanzhou 730050, China; sdweizhen0302@163.com

* Correspondence: 18297919986@163.com (D.W.); w120559779@163.com (Z.Y.)

Abstract: Roadway section form is an important part of the underground engineering structure, and it directly affects the overall stability of the roadway and the occurrence of underground disasters in coal mines. Based on this, this paper adopts a TYJ-500 electro-hydraulic servo rock shear rheology testing machine to conduct a uniaxial compression test on sandstone containing different prefabricated hole section morphology and analyzes the damage characteristics seen during the damage evolution process, with the help of a high-speed camera and acoustic emission monitoring equipment. The test results show that the pore morphology is the main factor affecting the mechanical parameters of sandstone, and the peak stress and elastic modulus of sandstone with pore sections have the characteristics of increasing and decreasing at the same time, except for the intact rock samples. The pore morphology exhibits central symmetry (circular holes and rectangular holes) damage, more pressure-shear cracks and shear cracks, and the acoustic emission characteristics of high-energy–low-amplitude–low-count of the “two low-trend and one high-trend characteristic curves” attributes; moreover, due to the special existence of its pore morphology, it leads to the rock samples having less energy accumulation and release. The axisymmetric hole types (trapezoidal holes and straight-wall domed holes) are damaged by tensile cracks and shear cracks, and their acoustic emission characteristics show the characteristic properties of “three high-trend characteristic curves” of high-energy–high-amplitude–high-count, and there is a strong elastic energy accumulation and output. The conclusions of this article can provide a certain theoretical basis for the design of coal mine roadway sections in underground structures, failure analysis, and stability evaluation of roadway structures.

Keywords: roadway section form; porous sandstone; fracture morphology; acoustic emission characteristics; energy evolution



Citation: Liu, G.; Wang, D.; Wang, S.; Zan, Y.; Zhang, Q.; Yang, Z.; Li, J.; Wei, Z. Effect of Sandstone Pore Morphology on Mechanics, Acoustic Emission, and Energy Evolution. *Buildings* **2024**, *14*, 3503. <https://doi.org/10.3390/buildings14113503>

Academic Editor: Guozhu Zhang

Received: 9 October 2024

Revised: 28 October 2024

Accepted: 30 October 2024

Published: 31 October 2024



Copyright: © 2024 by the authors. Licensee MDPI, Basel, Switzerland. This article is an open access article distributed under the terms and conditions of the Creative Commons Attribution (CC BY) license (<https://creativecommons.org/licenses/by/4.0/>).

1. Introduction

In the field of coal mining, the roadway is the main channel of coal resource mining and transportation, and the design of its cross-section pattern is not only related to mining efficiency, but also closely related to the safety of underground coal production. As an important part of the underground engineering structure, the roadway section pattern directly affects the stress distribution of the surrounding rock, the deformation characteristics, and the overall stability of the roadway, which is closely related to the occurrence of underground coal mine disasters [1–4]. Underground coal disasters, such as roof fall, coal and gas protrusion, impact pressure, etc., are the main safety threats in the process of coal

mining, and the occurrence of these disasters is often closely related to the irrational design of the roadway section pattern. For example, when the roadway section pattern cannot effectively disperse the surrounding rock stress, it can easily lead to the stress concentration phenomenon, increasing the risk of roof fall; in addition, some specific section patterns may also exacerbate the conditions of coal and gas protrusion, increasing the possibility of disasters. Therefore, an in-depth study of the relationship between roadway section morphology and the occurrence of underground coal disasters is of great significance for optimizing roadway design and improving the safety of coal mining.

Many scholars in China have produced a lot of research on the morphology of the roadway section. In the research of sandstone with a single-hole section, Yang Shengqi [5–7] and other scholars have studied the characteristics of crack initiation, expansion, evolution, and penetration of marble with a single hole under uniaxial compression, combined with a numerical simulation to analyze the effect of non-homogeneity on crack expansion, and found that the crack expansion pattern is significantly affected by the grain and its size. The experimental and simulation results are highly consistent with each other, and a more systematic description of the crack gradual evolution and microanalysis was carried out. Liu Zhaowei et al. [8] conducted an experimental study on the deformation and rupture process of a rock specimen containing a single circular hole under uniaxial compression and clarified that the localized deformation started at 80% of the axial displacement before the peak point and the deformation was the most intense near the peak point. They also found that the variation curve of the average maximum shear strain on the surface of the rock with the axial displacement reflected the evolution of the deformation and rupture of the rock. Zhou Junhua et al. [9] used a particle flow simulation program to conduct uniaxial compression tests on rock samples containing circular holes with different fracture morphologies and found that the fracture has a significant effect on the damage pattern of the hole-containing rock samples. They also found that fractures with different locations and characteristics change the formation of the main rupture zone, and that the damage modification coefficient ranges from 0.77 to 0.90. In the comparative experimental study of several holes, Li Guichen et al. [10] investigated the perimeter rock response of six roadway section shapes after rock excavation through numerical simulation and put forward the concepts of “equivalent excavation” and “ineffective reinforcement zone,” which emphasize the importance of section shapes on the distribution of the perimeter rock plasticity zone. The research of Du Mingrui et al. [11] goes deeper into the level of internal defects in rocks, especially the influence of hole geometry on the mechanical properties of sandstone. Through uniaxial compression tests and numerical simulations, the significant deterioration phenomena of bearing capacity and the elastic modulus of sandstone specimens containing holes were revealed, as well as the complex role of hole shapes on damage modes and crack extension characteristics. The study of Xu Lei et al. [12] explored the zonal rupture patterns and surrounding rock stability structure of different section shapes under equivalent excavation conditions through a combination of theoretical analysis, on-site measurements, and simulation analysis, and proposed a roadway stabilization principle that promotes the interdependence of multilayered load-bearing structures and joint load bearing. Gao Fuqiang et al. [13], on the other hand, used numerical calculations to directly compare the stability of the perimeter rock of the circular arch with that of the rectangular roadway, and emphasized the advantages of the circular-arch roadway in enhancing the stability of the perimeter rock. The study of Liu Gang et al. [14] focused on the local deformation and overall damage law of defective coal rock under bias loading, introduced the dynamic response analysis under bias loading conditions, and revealed the significant influence of the spatial arrangement morphology of the holes on the mechanical properties of sandstone through the bias loading test and acoustic emission monitoring of sandstone with the different morphology of three holes. Zhao Guoyan and Li Diyuan, on the other hand, carried out a detailed study on a variety of pore morphologies in order to further refine the effect of pore morphology on the mechanical properties of the rock. Zhao Guoyan et al. [15] systematically investigated the effects of circular, trapezoidal,

horseshoe, and square pores on the mechanical properties and fracture damage evolution law of red sandstone through uniaxial compression tests and digital image correlation techniques and deeply discussed the interaction mechanism between tensile cracks and shear cracks. Li Diyuan et al. [16] systematically analyzed the effects of circular, rectangular, trapezoidal, elliptical, and three-centered arch-shaped holes on the mechanical properties, damage modes, and crack extension characteristics of marble, revealing the relationship between the hole shape and the energy drop coefficient of brittle damage and the ejection intensity of the rock mass. They also further verified the experimental observations with numerical simulations to make clear the distribution of the stress and concentration characteristics of different hole shapes, which provides scientific information for an in-depth understanding of the damage mechanism of rocks. Lu Shasha et al. [17] analyzed the stress distribution range of three types of tunnels surrounding rock on the basis of theoretical research and carried out on-site verification.

Many scholars have focused on the mechanical properties of rock and their impact on the stability of underground engineering structures. Through experimental research, they have unveiled the mechanism of the stick–slip behavior in jointed rock masses as a source of rockbursts [18], investigated the load-bearing effect of prestressed anchor bolt structures and the mechanical properties of the surrounding rock [19], conducted a systematic analysis of the stress and deformation of the surrounding rock and support structures in ultra-large cross-section tunnels [20], explored in-depth the influence of natural discontinuities in hard rock on the deformation and failure mechanisms of deep rock [21], and studied the dynamic mechanical mechanisms and optimization methods for water injection into the roadway surrounding rock to prevent dynamic disasters [22]. Collectively, they have provided theoretical support for the design of underground engineering supports and offered new insights for the prevention of dynamic disasters in underground engineering.

In summary, the research on the roadway section in underground coal mines has been quite abundant, but further in-depth analysis of and discussion on the stability of the surrounding rock, the deformation characteristics, and energy evolution analysis for different section patterns are still needed. The previous research is not based on a certain coal mine roadway foundation, and the choice of hole morphology is also detached from the actual situation of the roadway cross-section morphology, while this paper is more skillfully derived from mechanical experiments regarding the underground structure of the roadway structural analysis and stability evaluation. Based on this, the author will carry out an in-depth study on the four common roadway section types, namely, circular, rectangular, trapezoidal, and straight-wall domed. By using a TAW-2000 electro-hydraulic servo rock shear rheology testing machine, combined with acoustic emission equipment, to conduct uniaxial compression tests on rock samples of the four types of prefabricated holes, the differences in the force characteristics, stress distribution characteristics, damage characteristics, and energy evolution laws of the different section types in underground engineering are analyzed. The research results are of great significance for improving the stability of the tunnel structure and preventing geological roof disasters.

2. Uniaxial Compression Damage Test of Different Holes

2.1. Test Equipment and Roadway Section Morphology Preparation

The test object adopted sandstone, conducted a non-metallic ultrasonic wave velocity test, and selected rock samples with relatively similar wave velocities. The raw rock samples were selected according to the requirements of the International Society of Rock Mechanics test specifications and procedures, with a size of 100 mm × 100 mm × 25 mm for the rectangular rock samples, using the center drilling method to prefabricate the type of roadway section. A complete specimen was used for the control of the test study. Three specimens were used in each group for the test, totaling 15 groups of tests. The effect of the four section types of fabrication and the arrangement are shown schematically in Figure 1. In order to ensure that there is only one single variable in the experimental study, it is required that the holes are located in the center of the rock samples, as much as

possible. In addition, in order to avoid the influence of the section area on the experimental results, and to only consider the different results due to the different morphology of the holes, it is required that the area of the prefabricated holes is kept consistent as much as possible (the area of holes was maintained at around 310 mm²). We extended the coal mine roadway section form area consistency, thereby ensuring the consistency of the mine in transportation, ventilation, and other functions. The inner diameter of the circular section was 20 mm, the length of the rectangular section was 20 mm, the width was 15 mm, the semi-circular diameter of the straight-wall arched section was 15 mm, the length of the bottom was 15 mm, the width was 15 mm, and the trapezoidal section had an upper bottom of 10 mm, a lower bottom of 20 mm, and a height of 20 mm. The specific specimens and the dimensions of the holes preformed are shown in Table 1 below.

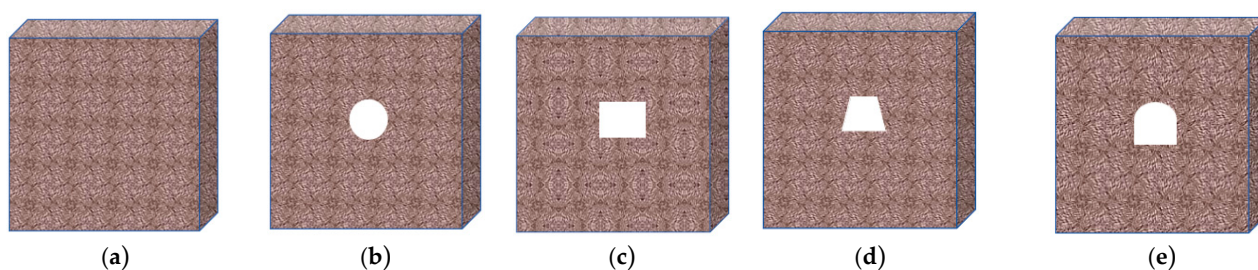


Figure 1. Prefabricated roadway cross-section morphology sandstone specimen. (a) Complete rock sample; (b) orbicular; (c) rectangular; (d) trapezoidal; (e) straight-wall domed form.

Table 1. Specimen form and dimensions.

Specimen Number	Hole Patterns	Hole Pattern and Its Size/mm	Hole Area/mm ²
WZ-YY-01	Complete rock sample	/	0
WZ-YY-02	Complete rock sample	/	0
WZ-YY-03	Complete rock sample	/	0
YX-DM-01	Orbicular	Calibre: 19.86	309.78
YX-DM-02	Orbicular	Calibre: 20.01	314.47
YX-DM-03	Orbicular	Calibre: 19.92	311.65
JX-DM-01	Rectangular	Length: 20.21, Width: 15.28	308.81
JX-DM-02	Rectangular	Length: 20.25, Width: 15.22	308.21
JX-DM-03	Rectangular	Length: 20.16, Width: 15.24	307.24
GX-DM-01	Straight-wall domed form	Semicircular diameter: 15.12, Underneath: 15.10, Width: 15.12	318.19
GX-DM-02	Straight-wall domed form	Semicircular diameter: 15.02, Underneath: 15.06, Width: 15.04	315.10
GX-DM-03	Straight-wall domed form	Semicircular diameter: 15.04, Underneath: 15.01, Width: 15.03	314.43
TX-DM-01	Trapezoidal	Upper bottom: 10.23, Underneath: 20.21, Height: 20.05	305.71
TX-DM-02	Trapezoidal	Upper bottom: 10.13, Underneath: 20.26, Height: 20.17	305.90
TX-DM-03	Trapezoidal	Upper bottom: 10.08, Underneath: 20.17, Height: 20.18	305.58

2.2. Test Method

The test was conducted using the loading device for the TAW-2000 microcomputer control electro-hydraulic servo universal testing machine. The test system can perform a real-time recording of the specimen loading process of force and displacement data, through the supporting analysis software, which can be obtained from the stress–strain data test loading end and the control system, as shown in Figure 2. The test adopted a displacement-controlled loading mode, where the loading rate was 0.02 mm/s. A high-speed camera was used to collect the whole process information of the sandstone specimen from contact to compression density until the final destabilization and destruction of crack germination and development to the final penetration. We can also conduct real-time monitoring of the whole process of sandstone stress–strain data with the stress–strain acquisition device. With

the help of the acoustic emission instrumentation, used to detect acoustic signals during the whole process of the test, we can show their time–space and time–strain data during the rupture gestation process and their spatial and temporal distribution during the rupture brewing process. The threshold was set to 100 dB to eliminate the high signal-to-noise ratio. The acoustic emission probe was fixed to the middle part of both sides of the specimen with a rubber strap, while a petroleum jelly reagent was used to couple the acoustic emission probe to the specimen.

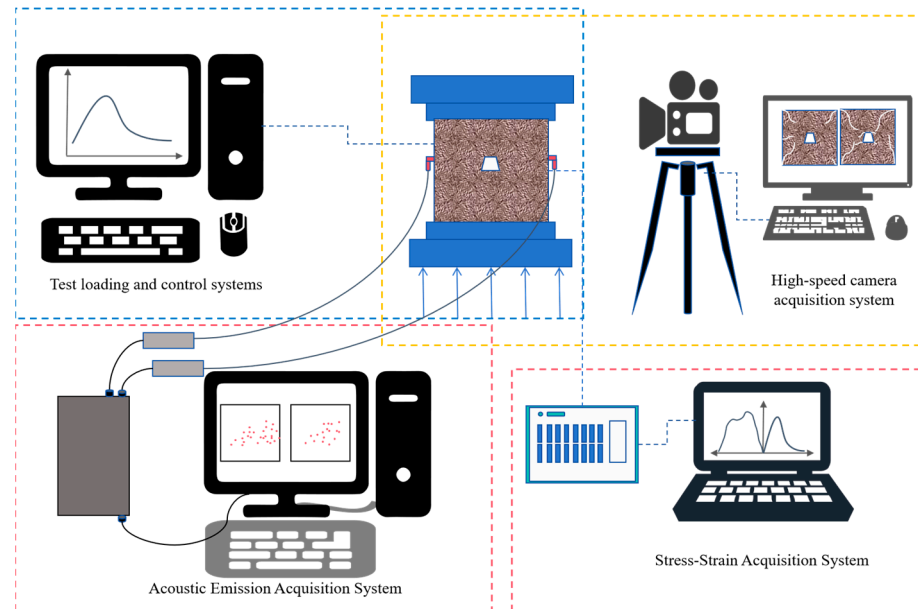


Figure 2. Experimental test system.

By analyzing the stress–strain curves of the four section morphologies and the intact sandstone specimens, as shown in Figure 3 below, the data of the ultimate compressive strength, peak displacement, and modulus of elasticity of the prefabricated sandstones with different section morphologies under uniaxial compression were obtained, as shown in Table 2.

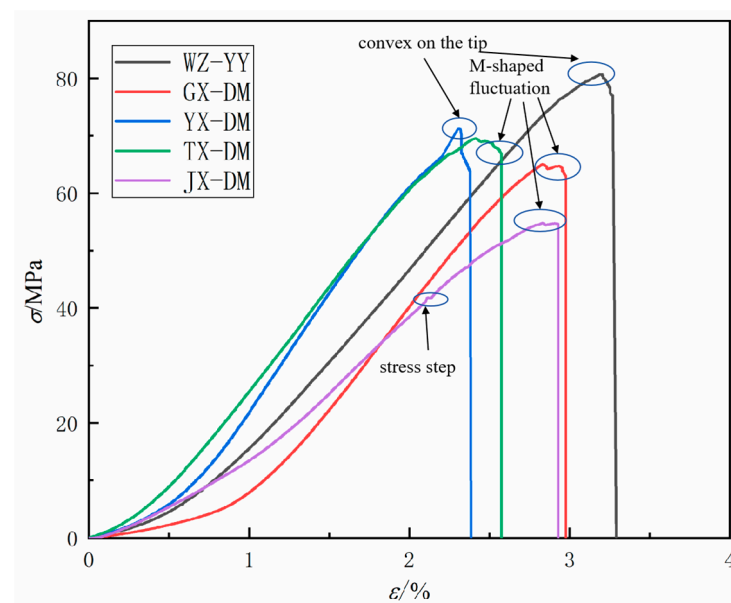


Figure 3. Full stress–strain curves for sandstones with different pore morphologies.

Table 2. Mechanical parameters of sandstone specimens with different pore sections.

Specimen Number	σ_{max}/MPa	$\epsilon_{max}/\%$	E/GPa
WZ-YY	81.48	0.38	41.22
YX-DM	72.03	0.23	38.95
JX-DM	54.89	0.28	27.42
GX-DM	66.60	0.29	36.99
TX-DM	70.10	0.24	36.27

The stress–strain curves of the rock samples with different cross-sectional morphologies are shown in Figure 3. Upon observing the curves, it is evident that, regardless of the preformed hole cross-sectional morphology in the samples, there exists a noticeable crack compaction stage. However, when considering the duration of the compaction stage, the straight-wall circular-arch cross-section and the circular-hole cross-section both experience significantly longer compaction stages compared to the other three types of hole-containing rock samples. This can be attributed to their unique hole shapes, which cause the stress to be transmitted downward along the curved upper surface in “raindrop-like” dispersion, requiring more time for stress transmission and facilitating energy concentration and storage. The shape of the holes also influences the energy evolution of the rock during compression. In the early stages of compression, the rock primarily absorbs energy and undergoes elastic deformation. As the uniaxial compression test progresses, the rock surrounding the holes exhibits different energy absorption rates and release characteristics, due to the varying shapes. The circular holes, with their relatively uniform shape, transmit stress to the lower part in a circular-arch pattern, resulting in a relatively stable energy absorption and release process. In contrast, the straight-wall circular-arch, trapezoidal, and rectangular holes, due to their linear structures in the lower part, may experience sudden changes in energy release caused by local stress concentrations and secondary damage, leading to noticeable fluctuations in the stress–strain curve. This results in a more significant “M”-shaped wave pattern at the peak failure point for the rectangular-, arch-shaped, and trapezoidal-hole cross-sectional sandstone samples. Conversely, the intact rock samples and the circular-hole cross-sectional samples accumulate energy and then exhibit a large tip protrusion at peak failure, causing a substantial one-time energy release. From the curves, it can be observed that, during the initial compaction stage, the rectangular cross-section curve rises rapidly in an upward parabola, while the intact rock, arch cross-section, circular-hole cross-section, and trapezoidal-hole cross-section curves rise in a downward parabola, with a slower ascent. At the same time, the different cross-sectional morphologies have varying degrees of impact on the curve’s drop and the shift of the peak yield point.

Overall, all of the types of hole-containing sandstone samples exhibited a typical deformation pattern, transitioning from plasticity to elasticity, and then back to plasticity during the stress process. In the initial stage of deformation, the sandstone samples with different hole morphologies showed distinct crack closure stages. The samples with linear boundary holes (rectangular, arch-shaped, and trapezoidal cross-sections) had more microcracks (more fluctuations), while those with curved-hole cross-sections (circular and straight-wall circular-arch cross-sections) had fewer curve fluctuations, instead showing instantaneous brittle failure with tip protrusion. The reason for this lies in the special curved structural cross-section, which allows the vertical load to be distributed uniformly, thereby slowing down the damage process. When the peak stress is subsequently reached, significant brittle failure occurs immediately. In addition, when transitioning from the crack compaction stage to the elastic stage on the rectangular cross-section curve, a noticeable stress step phenomenon appears, indicating that the rectangular-hole cross-section samples will experience more intense failure. Furthermore, in the post-peak stage, they mostly exhibit strain-softening plastic failure characteristics.

A comparison of the peak failure strength and the elastic modulus for the different cross-sectional shapes is shown in Figure 4. As can be seen from the figure, the relative errors of the elastic modulus among each group of samples with circular, trapezoidal,

straight-wall circular-arch, and rectangular shapes are all relatively small, indicating that the selected samples are mostly homogeneous in texture and similar in internal pore structure and distribution. Compared with the intact samples, the average peak compressive strengths of the circular, trapezoidal, straight-wall circular-arch, and rectangular cross-sectional hole samples were 88.40%, 86.03%, 81.74%, and 67.37% of the average peak compressive strength of the intact rock, respectively. The experimental data show that the circular cross-sectional hole had the lowest weakening effect on the compressive strength of the sandstone samples in terms of structure, with only an 11.6% reduction compared to the ultimate compressive strength of the intact rock samples, while the rectangular cross-sectional hole led to the most significant strength reduction, with a decrease of 32.63%. This is because, when the circular hole is subjected to force, the stress distribution is relatively more uniform, due to the symmetry of its shape. This uniform stress distribution helps to reduce local damage to the sample during compression, thereby delaying the overall failure process. The circular hole has no sharp edges, so it is less prone to stress concentration. Stress concentration is one of the important factors leading to material failure, and the design of circular holes effectively reduces this risk. Square holes are more prone to stress concentration at their sharp edges. Stress concentration can cause local stress to exceed the material's strength limit, leading to crack propagation and sample failure. This failure often occurs at lower stress levels, so square holes have a more severe weakening effect on the compressive strength of the samples. A square hole creates a relatively larger material discontinuity in the sample. This discontinuity can lead to uneven stress distribution around the hole, further exacerbating the stress concentration phenomenon. At the same time, this discontinuity also provides a path for crack propagation, reducing the overall strength of the sample.

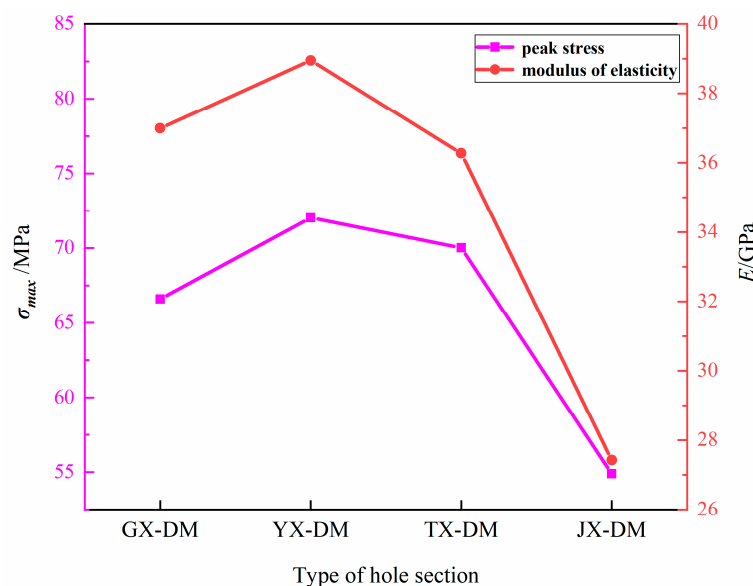


Figure 4. Peak stress versus modulus of elasticity data for the different hole specimens.

Further analysis of the peak strengths of the sandstone samples revealed the following pattern: the circular-hole samples exhibited a relatively high peak strength of 72.03 MPa; followed by the trapezoidal and straight-wall circular-arch samples with peak strengths of 70.10 MPa and 66.60 MPa, respectively; while the rectangular hole samples had the lowest peak strength of only 54.89 MPa. Similarly, a comparable trend was observed in the comparison of the elastic moduli, where the circular-hole samples had the highest elastic modulus of 38.95 GPa, followed by the trapezoidal and straight-wall circular-arch samples, with the rectangular hole samples having the lowest elastic modulus of just 27.42 GPa. This demonstrates that the prefabricated hole defects significantly weaken the compressive strength and deformation characteristics of the rock samples. The different types of samples

showed similar trends in peak strength and elastic modulus, and it is evident that the elastic modulus and the peak stress of the samples with different hole cross-sections exhibited concurrent increases or decreases.

On the other hand, it is clear that the arc-shaped holes (such as the circular holes) performed superiorly in terms of their load-bearing capacity and material stiffness, while the mixed arc and straight-line holes (such as the straight-wall circular-arch holes) fell in the middle range. In contrast, the fully straight-line holes (such as the rectangular and trapezoidal holes) exhibited poorer mechanical properties. Given that all of the samples in the experiment were highly consistent in size, hole position, and cross-sectional area, with only the hole shape being set as an independent variable, it is evident that hole shape is a crucial factor influencing the mechanical properties of sandstone samples. In the design of roadway cross-sections in underground coal mines, selecting trapezoidal or straight-wall circular-arch cross-sections is more conducive to the stability of the roadway and can, to a certain extent, delay the occurrence of disasters.

3. Analysis of Crack Progressive Damage Process Under Uniaxial Compression

Grasping the rupture characteristics of rock samples with different section patterns is of great significance for the control of the surrounding rock stability and disaster prevention, so the derivation and rupture characteristics of cracks and crack types of prefabricated pore patterns under uniaxial action are discussed and analyzed here. In order to quantitatively analyze and identify the secondary crack extension process and its fracture type (e.g., tensile, shear, or compressive shear modes) in the porous sandstone specimens under uniaxial compression conditions, we have illustrated (in Figure 5) the typical macroscopic damage pattern of sandstone with porous fractures during uniaxial compression. The letter markers in this illustration are intended to distinguish the different types of crack extension, while the corner numbers represent only the chronological order of the crack appearance.

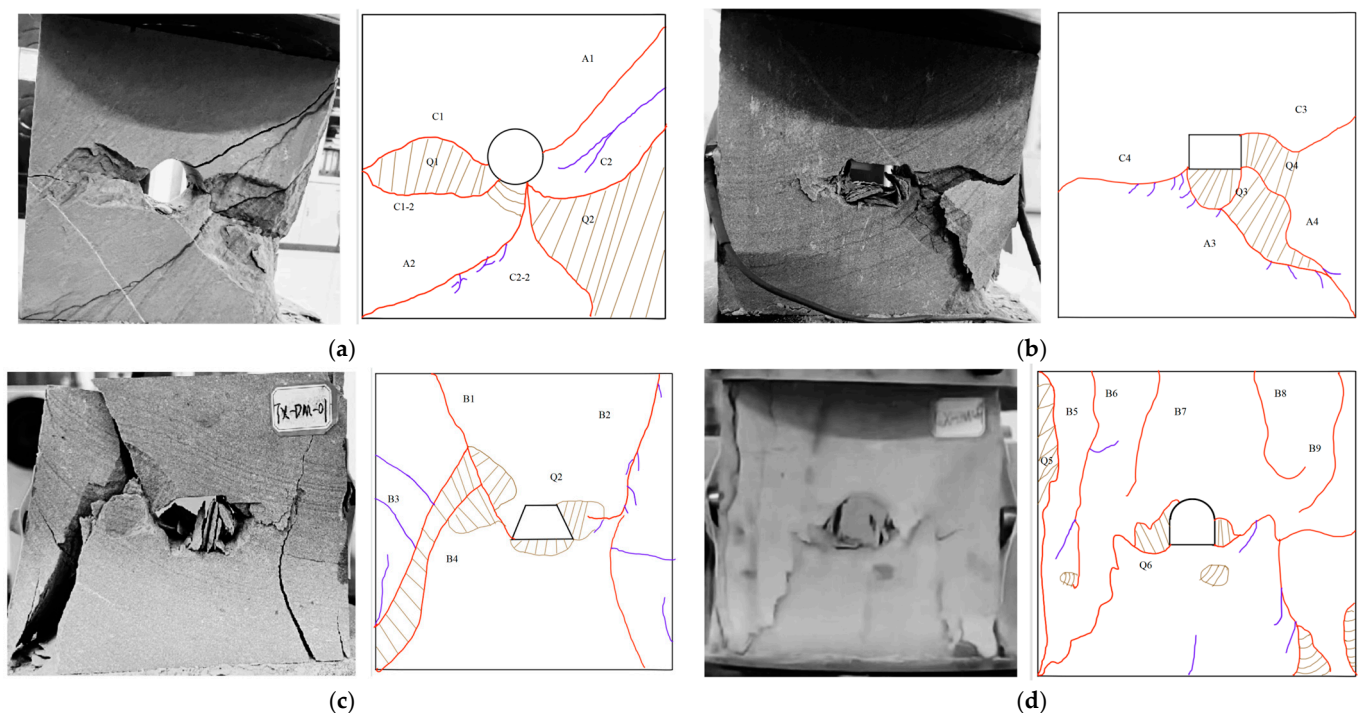


Figure 5. Schematic diagram of progressive damage in sandstone with different pore patterns. (a) Orbicular form; (b) Rectangular pattern; (c) Trapezoidal pattern; (d) Straight-wall domed form.

The different mechanisms of crack formation can be categorized into the following three types: tensile cracks, shear cracks, and compressive-shear cracks. Tensile cracks can be divided into two kinds, as follows: one kind of tensile crack is distributed at the top and

the bottom of the hole section, which are the two regions with more concentrated tensile stresses; and the other kind of tensile crack is distributed along the vertical laminations, which is the tensile damage of the laminations. The shear cracks started in the compressive stress concentration area on both sides of the hole and gradually developed to the far side under continuous loading, and the failure modes of the specimens mainly covered the following three types: the collapse of the inner wall of the hole, the initial formation and expansion of the cracks, and the peeling and fragmentation of the surface material. These failure modes are closely related to the specific morphology of the hole cross-section in the specimen, and the different morphologies of the holes lead to significant differences in the degree of inner wall collapse.

Figure 5 presents the failure modes of the sandstone samples with different hole sections under uniaxial compression. The macroscopic failure characteristics of the samples mainly include hole-wall collapse, crack propagation and extension, and surface spalling damage. According to Zhu Tantan et al. [23], based on the generation mechanism of secondary cracks, shear-dominated cracks occur when the shear strength of the rock is overcome during crack propagation, causing the crack to propagate along a shear plane. During crack propagation, acoustic emission phenomena may accompany this process, due to the sudden decrease in the internal energy of the rock caused by the release of shear stress. The failure mode of the rock may manifest as shear failure, such as splitting failure or sliding failure along a certain plane. Tensile-dominated cracks occur when the tensile strength of the rock is overcome during crack propagation, leading to crack propagation occurring along the tensile direction. Crack propagation typically exhibits sudden brittle fractures, because tensile stress can quickly reach the strength limit of the rock. The failure mode of the rock may manifest as tensile failure, such as a tensile fracture or tearing along a certain direction. Compressive-shear cracks, which are jointly dominated by both shear and tensile stresses during crack propagation, result in complex and varied crack paths. The failure mode of the rock may manifest as composite failure, incorporating characteristics of both shear and tensile failure. The acoustic emission phenomena may be more complex because the combined action of shear and tensile stresses leads to multiple releases and the redistribution of internal energy within the rock. Drawing on the research experience of previous scholars and combining the specific samples in this experiment, the crack types can be specifically subdivided into three categories, A, B, and C, each with unique characteristics and evolution laws, as follows:

Category A cracks (shear-dominated cracks): These cracks originate from the areas formed by hole wall collapse on the left and right sides of the prefabricated holes. Their propagation paths trend diagonally upward or downward, typically manifesting as inclined main cracks with two wings penetrating the sample surface. The surrounding hole walls gradually collapse, ultimately leading to the formation of fracture surfaces, indicating the concentration and release of shear stresses within the rock samples containing holes.

Category B cracks (tensile-dominated cracks): These cracks originate from the destruction of the upper and lower hole walls within the central range of the sample under tensile stress. The initial propagation direction is mostly along the axial loading path. However, due to the heterogeneity of the rock material and the stress concentration effect at the ends of the sample, the Category B cracks may deviate from the original axial direction during the later stages of propagation, exhibiting more complex path changes. On the surface of the rock sample, macroscopic cracks parallel to the stress application direction are formed, causing certain tensile and tearing effects in the vertical direction.

Category C cracks (compressive-shear composite cracks): The formation of these cracks is closely related to the overall instability of the sample, manifesting as the structural transverse fracture of the rock sample containing holes. Their appearance is generally delayed compared to Category A and B cracks. They are the ultimate manifestation of the loss of structural integrity of the sample under complex stress conditions, especially with the combined action of compressive and shear stresses. The direction of the compressive-shear composite cracks on the sample surface usually has a certain angle with the stress direction

of the sample. This is because, under composite compressive-shear stress conditions, the crack propagation direction is jointly influenced by normal stress and shear stress. Macroscopically, compressive-shear composite cracks may manifest as obvious crack lines or crack zones, which may penetrate the entire sample or only appear locally on the sample surface. Microscopically, crack propagation paths may exhibit features such as tortuosity, bifurcation, or propagation along the grain boundaries.

There is a significant difference between the fracture mode and the fracture characteristics of the pore-bearing sandstone rock samples. As shown in Figure 5a, during the axial loading of the sandstone samples with circular holes, two macroscopic shear cracks (A1 and A2) are generated around the holes that are close to the diagonal angles along the left and right sides of the holes, under the action of the holes. The reason for analyzing this factor is that, when the loads are transmitted downward, the circular holes cause stress concentration, which results in greater stresses on the material around the holes, and the loads select the weakest point. When “attacking” the lower rock sample, the end position was chosen first, which led to a cracking stress of 25.2 MPa at the right end of the circular-hole specimen. The stress then continues to conduct downward in the process due to the specificity of the circular specimen morphology. In the specimen on the left and right sides of the formation of more symmetrical compression, as well as in shear cracks C1 and C2, a starting stress of 35.7 MPa is observed, which gradually moves to the specimen on the lower end face of the development of the main cracks to generate secondary cracks C1-2 and C2-2 before shear crack A2 cracking and expansion. When they continue to load, the cracks expand rapidly to the end face expansion, the main crack formation of through stress falls violently, the material begins to show fatigue damage and spalling regions Q1 and Q2.

Comparing the final damage pattern and the damage sequence of the sandstone samples with different pore morphologies, it was found that the damage characteristics of the two types of pore samples, circular and rectangular, are the same as those of the two types of pore samples that are symmetrically distributed up and down in morphology, as shown in Figure 5b. It can be observed that, in the rectangular pore samples, the initial shear zones C3 and C4, which were formed on the left and right sides of the holes with an angle of 45 degrees from the loading direction, were formed in the vicinity of the main cracks and secondary cracks A3 and A4 gradually when the load continued to be transmitted downward. As the load continues to be transmitted downward, secondary cracks A3 and A4 are formed in the vicinity of the main cracks, and large-scale debris spalling zones Q3 and Q4 are formed around the hole due to the through stress damage of the main cracks and the secondary cracks. When analyzing the morphology of the sample with the symmetry between the circular and rectangular shapes in the horizontal direction, compressive-shear cracks appear symmetrically on the left and right sides of the hole when the sample is subjected to the uniaxial compression test. The reason for this may lie in the special nature of the mathematical shape of the holes, where the main stresses on the rock samples are applied along the vertical direction, but additional shear stresses may be generated around the holes. These shear stresses are the main cause of the formation of cracks, especially if there are defects or weaknesses in the surface of the specimen, when the number of compressive-shear cracks becomes more evident.

It can be observed that the crack derivation patterns of the trapezoidal-hole and straight-wall domed hole specimens are well characterized by symmetrical damage along both sides of the main axis. As shown in Figure 5c, firstly, the stress on both sides of the trapezoidal-hole specimen is transmitted downward, which then produces two larger tensile cracks (B1 and B2), and, at the same time, due to the specificity of the two bottom corners of the trapezoidal shape, it has a certain rupture-inducing effect on tensile crack B2, and then reaches the crack-initiating stress of 27 MPa on the left side, which produces two more obvious tensile cracks (B2 and B3) on the left side of the rock sample. Thereafter, the local stress of the specimen reaches 27 MPa. Here, the local stress of the specimen reaches its stress limit, and microcrack penetration damage produces a crushed spalling zone in the right middle region of the specimen. Similar to the trapezoidal shape, the straight-wall

domed specimen produces multiple more uniform tensile cracks (B5, B6, B7, B8, and B9) in the upper part of the specimen at the early stage of compression, and, at the same time, the initial cracks on the left side of the hole cross-section also extend approximately along the direction of the expansion of the original cracks in a tensile damage pattern toward the loaded end face to form crack-breaking surface Q5.

Compared with the first three holes, the damage process of the straight-wall domed hole is gentler, as shown in Figure 5d, only in the compression process at the end of the surface, where a small amount of fragmentation occurs. In addition, the stress in the search for the optimal unloading path along the edge of the hole form unloads, due to the stress relief brought about by the significant crack rupture surface Q6, as well as in the macroscopic crack extension. At the same time, there are varying degrees of rock debris fall with crisp sound along the macrocrack expansion path. As in the case of the trapezoidal holes, due to the special position of the two bottom corners of the dome shape, the optimal unloading path after stress transfer to the periphery of the holes is also determined to be in the diagonal transfer of the two bottom corners to the bottom of the rock samples.

The comparative analysis of the rupture morphology of the rock samples containing different pore morphologies is mainly manifested in the different types of cracks appearing, with the centrosymmetric pore types (circular pore and rectangular pore) showing more compressive-shear cracks and shear cracks, while the axisymmetric pore types (trapezoidal pore and straight-wall domed pore) show more tensile cracks and shear cracks.

In the uniaxial compression failure mechanism of brittle rocks, the variability mainly originates from two aspects, as follows: one is the difference in the pore morphology and its geometric characteristics, and the other is the inherent inhomogeneity of the rock materials. From a macroscopic perspective, the final damage of the rock is the result of the gradual accumulation and evolution of the micro-damage in the early stage, in which the main manifestation of the early damage is the local microcracks induced by the stress concentration at the edge of the prefabricated holes.

When comparing the macroscopic fracture patterns of the different specimens, it can be clearly observed that the course of crack initiation is expansion until penetration is highly consistent with the dynamic evolution of the principal strain field on the fine-scale. Specifically, crack development is a dynamic process, accompanied by the continuous expansion of the high-strain region, during which microscopic ruptures continue to sprout, develop, and eventually converge into a nucleus to form a macroscopically visible crack system. This process reveals the close connection between the micro-mechanism of rock damage and the macro-expression, i.e., the macro-damage is the final manifestation of the accumulation and evolution of the micro-damage.

4. Characterization of Acoustic Emission Under Uniaxial Compression

From the schematic diagrams combining acoustic emission (AE) characteristic parameters with stress–strain curves for four different cross-sectional shapes provided in Figure 6, it is evident that, during the initial contact between the circular and trapezoidal specimens with the press ram, there was no significant acoustic signal in the AE event count during the compaction stage of the curve, resulting in a notable blank window period. As the rock samples entered the nonlinear deformation stage, the axial stress–strain curve gradually deviated from a straight line and rose slowly and uniformly. A substantial number of AE events occurred in the single-hole sandstone samples with different cross-sectional shapes, and the number of AE activities increased significantly. The peak energy of the circular-hole specimen reached 762,000 aj, the peak amplitude reached 87 db, and the limit ring-down count even reached 12,218. For the trapezoidal-hole specimen, the peak energy reached 743,695 aj, the peak amplitude reached 86 db, and the limit ring-down count reached 32,128. This phenomenon indicates that the brittle sandstone is about to undergo instability and failure. Both the circular- and the rectangular-hole cross-sectional sandstone specimens generated a small number of AE signals during the initial compaction stage. The reason for this is that real rock masses have some degree of initial primary rock damage, which results

in the production of certain AE events. Observing the four images clearly shows that many AE events are concentrated around potential tensile damage zones. Therefore, the pores and fractures within the rock are the causes of cracks in the sandstone specimens. The tensile fracture zone ultimately reaches the vertical upper and lower boundaries. In contrast, the rectangular-hole cross-section exhibits a relatively obvious characteristic failure point during the initial compaction stage. Subsequently, the AE signals showed a relatively prolonged period of inactivity. According to the analysis by scholars [24], the reason for this is that, during the initial stage, the press ram causes some acoustic signals due to the internal particle compression and collision resulting from the accumulation of relatively hollow material within the rock sample. Then, the specimen enters the elastic yield stage. Due to the uniqueness of the rectangular hole shape, there are not many AE signals in the early stage, leading to the emergence of the inactive period.

The locations of acoustic emission (AE) events for the specimens with straight-wall circular-arch-shaped hole cross-sections during uniaxial compression are shown in Figure 6a. It is clearly visible that, when the vertical stress reaches around the critical stress value, the AE events are predominantly concentrated around the perimeter of the cylindrical cavity. The AE events are mainly focused on the upper and lower surfaces of the circular hole in the upper half, gradually forming clusters, which initiate tensile and shear fractures. Although many AE events are recorded outside of the rock mass region surrounding the cavity, these AE events do not represent active microcracks. In the initial stage, it is difficult to predict the initiation location of macroscopic cracks during loading, because the AE events are discrete within the specimen. The AE active zones connect to form a large AE active area, with the quantity levels of AE characteristic parameters having a limit energy of 572,933 aj, a limit amplitude of 79 db, and a peak ring-down count of 19,501, which correspond to the locations of the macroscopic cracks. In contrast, during the entire loading process, local AE events rarely occur in the region near the cavity wall.

Under the influence of strong interactions between isolated microcracks, these isolated microcracks gradually expand in an unstable manner, resulting in a U-shaped fluctuating growth tendency, which eventually merges to form split macrocrack damage. Tensile cracks begin to appear in the top bottom plate of the domed cavity. With the increase in axial load, the tensile cracks gradually expand, nucleate, and agglomerate, and, thus, the rock sample is destabilized, and the tensile cracks sprout and develop from the top and bottom plates. With the increase in compressive stress, cracks begin to appear near the termination point of tensile fracture and at a certain distance from the cylindrical cavities of the top and bottom plates, and the cracks expand parallel to the direction of the axial stress, appearing in the period of extremely rapid activity of the AE, and eventually causing damage to the specimen. On the contrary, the circular-hole section with the same curved upper edge, in the elastic yielding stage, is not as “enthusiastic” as the signal of the circular-arch section, due to the fact that it is not easy to form stress concentration at the top. In addition, the stress is uniformly dispersed to the top of the various parts, resulting in the amplitude of the absolute energy and ringing counts being in the way of the stress–strain curve characteristics of the upward throwing shape, which slowly rises until the sample is broken. The stress–strain curve is characterized by a slow upward throw until the rock sample is broken. Turning to the trapezoidal pore samples, the number of acoustic emission events is limited, and the trend is smooth at the initial stage of press loading when the load is at a low level. However, a significant increase in the acoustic emission signals was observed at a time point of about 50 s. This phenomenon can likely be attributed to the sudden destabilization of the localized areas (e.g., at pores or micro-defects), due to the uneven distribution of stress within the sample, which is manifested as localized collapses or micro-fractures on the surface. This phase is still defined as a compaction phase, characterized by the fact that the microcracks within the sample have not yet expanded significantly, and, therefore, the overall level of acoustic emission activity remains relatively low.

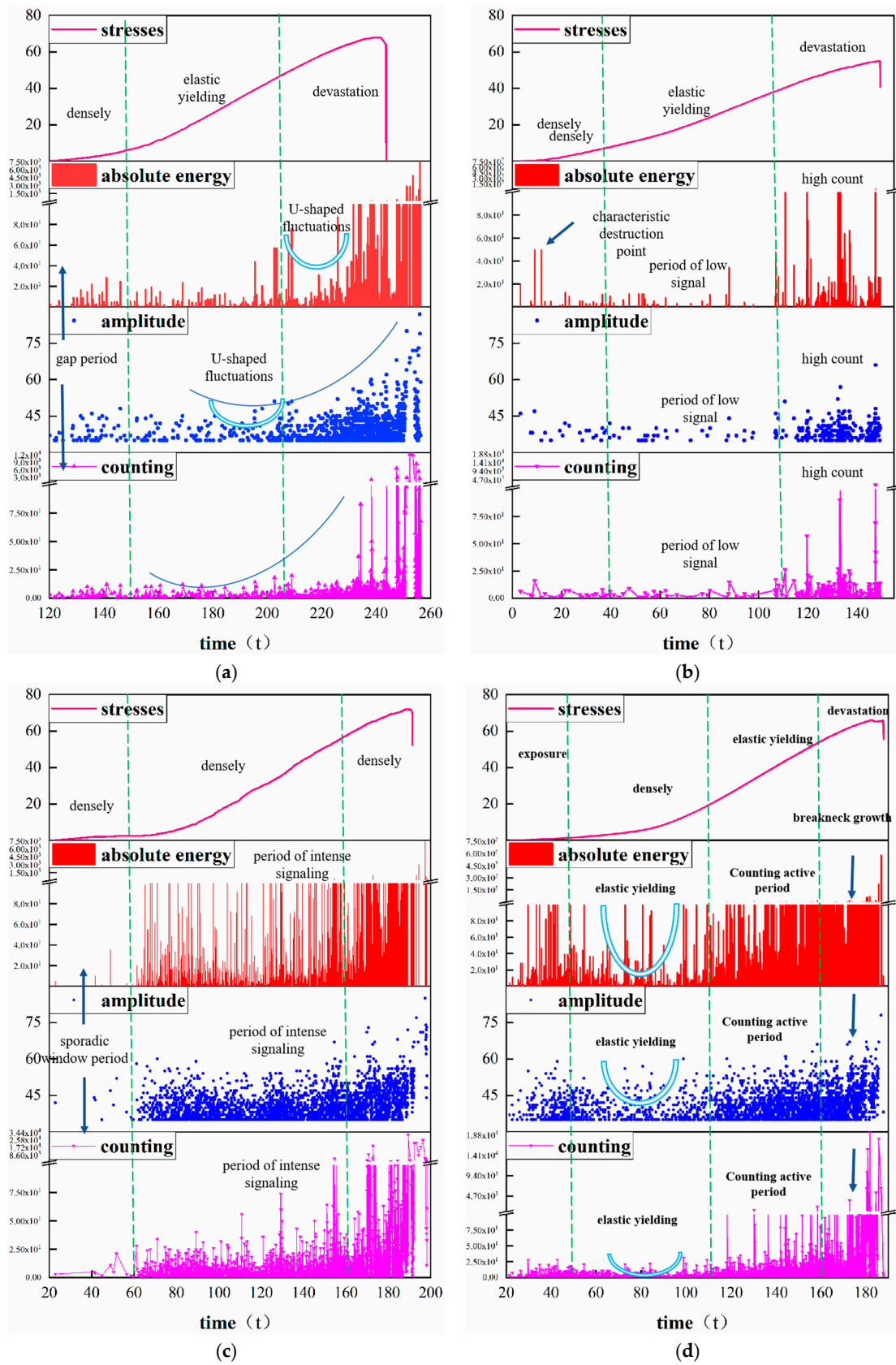


Figure 6. Schematic characterization of acoustic emission events of the rock samples from different hole sections. (a) Orbicular form; (b) Rectangular pattern; (c) Trapezoidal pattern; (d) Straight-wall domed form.

To comprehensively analyze the AE events (stress-absolute energy-amplitude-ringer counts), diagrams of sandstone with four different pore section morphologies were created, according to the law analyzed in Section III, which show the acoustic emission characteristics of the axisymmetric-shaped pore (straight-wall domed and trapezoidal). They show the characteristic attributes of high energy, high amplitude, and high counts, referred to as the “three highs.” The acoustic emission characteristics of holes (circular and rectangular) in a centrosymmetric shape show the characteristic attributes of high energy, low amplitude, and low counts, referred to as high-energy–low-amplitude–low-count, which are “two lows and one high.” In terms of a local comparison, from the specimen-loaded stress curve and acoustic emission ringer counts, the acoustic emission energy curve correspondence can be seen, the stress occur suddenly, and the drop acoustic emission ringer counts and acoustic emission energy appear as a surge phenomenon, but ringer counts surge and acoustic emission energy show a surge phenomenon, and the stress curve does not necessarily show sudden drop changes, and, at the same time, we observed the sandstone specimen before the peak stress. At the same time, observing the “silent period” before the peak stress and the “silent period” of acoustic emission parameter changes, it can be clearly found that the “silent period” of acoustic emission parameter changes does not mean that the destructive deformation field of the rock is in a stable stage, however, in the peak stress of the specimen, the stress curve does not necessarily undergo a sudden drop. On the contrary, in the “quiet period” before and after the peak stress of the specimen, the acoustic emission parameters have more obvious violent fluctuations, according to the research of Song Yimin et al. [25], due to the localization of the deformation during this period brought about by the size of the specimen and the value of the obvious increase.

5. Analysis of Energy Evolution Laws

Many scholars have jointly focused on wave propagation in media, energy evolution during rock failure processes, and the dynamic properties of materials. Xu et al. [26] investigated the influence of nonlinear barriers on the wave propagation in saturated soil systems, providing a new perspective for understanding wave propagation characteristics. Feng et al. [27] delved into the delayed failure process of granite, along with its energy evolution and acoustic emission characteristics, offering significant data support for the study of rock failure mechanisms. These studies have not only enhanced our understanding of wave propagation, failure mechanisms, and material properties in rocks and soils, but have also provided theoretical support for disaster prevention and mitigation in related engineering fields. The deformation and breakage of rocks is essentially an energy dynamic conversion process, which involves both the accumulation of elastic strain energy and the gradual dissipation of energy. In particular, the common interlayer structures in rocks show obvious directional differences in energy storage and release, due to the different directions of force application, resulting in their deformation and damage behaviors. This anisotropic property of energy release plays a crucial role in assessing the stability of engineering structures during deformation.

Based on the theoretical framework of energy dissipation and release proposed by scholars, as well as the energy-driven damage and rupture mechanism [28–32], we can see that rocks undergo a complex energy flow process when they are subjected to compression and deformation until destruction, as follows: from external energy input, to the gradual accumulation of releasable elastic strain energy, to the continuous dissipation and release of such energy through different forms. If we envision an independent system with closed energy, the rock unit undergoes deformation and damage under the action of external force, and, according to the basic principle of energy conservation and conversion, there exists a dynamic equilibrium and conversion relationship between the different forms of deformation energy [33–35], as shown in Figure 7. In addition, because there is no peripheral pressure, the whole test involves only the unidirectional energy input of axial load; moreover, through the integral operation of the stress–strain curve, the change in

strain energy in each stage can be directly calculated, and the integral schematic is shown in Figure 8. The mathematical relationship between the energies is as follows:

$$U = U^e + U^d \tag{1}$$

Among them,

$$U = \int_0^{\varepsilon_1} \sigma_1 d\varepsilon_1 \tag{2}$$

$$U^e = \frac{1}{2} \sigma_1 \varepsilon_1^e = \frac{1}{2E_u} \sigma_1^2 \tag{3}$$

The rock samples were put under uniaxial compression without an unloading process, but due to the elastic response of the rock, its elastic modulus in the loading and unloading process to maintain a relatively stable consistency of the slope of the curve is approximately the same. Therefore, Equation (3) can be changed to the following:

$$U^e = \frac{1}{2E} \sigma_1^2 \tag{4}$$

$$U^d = U - U^e \tag{5}$$

In the formula, the following applies:

U is the total strain energy, kJ/m^3 ; U^e is the elastic strain energy, kJ/m^3 , U^d is the dissipated energy, kJ/m^3 ; σ_1 is the axial stress, MPa; ε_1^e is the elastic strain; E is the loaded elastic modulus, MPa; and E_u is the unloaded elastic modulus, MPa.

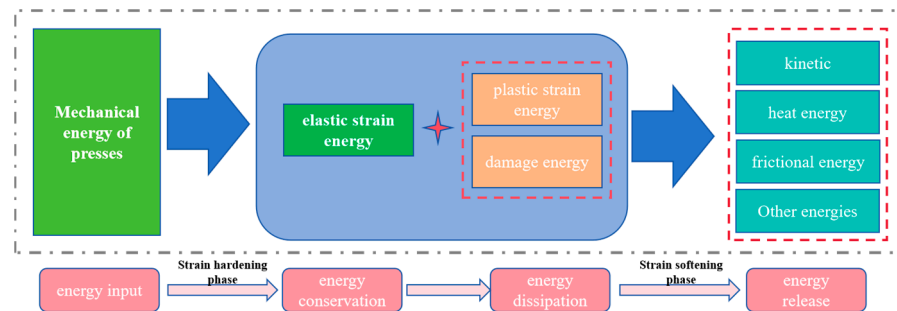


Figure 7. Schematic diagram of energy transfer in the internal system of the loaded coal rock mass.

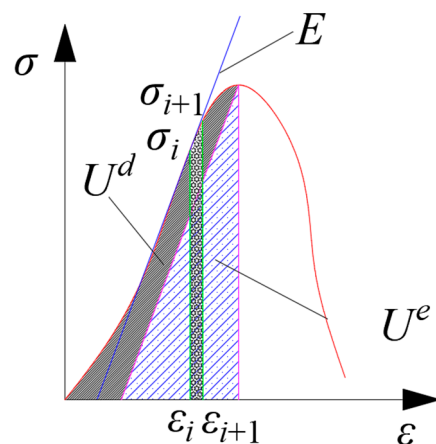


Figure 8. Calculation method of energy conversion of the stress–strain curve.

In uniaxial compression tests, the mechanical energy input to the press is mainly converted into the elastic strain energy, plastic deformation energy, and thermal energy of the specimen [36,37]. Specifically, as the stress increases, the specimen first undergoes

an elastic deformation stage, at which time the input energy is mainly converted into elastic strain energy within the specimen, which is stored in the form of potential energy in the microstructure of the material. When the stress exceeds the elastic limit of the material, the specimen enters the plastic deformation stage, at which time the input energy continues to be converted into elastic strain energy, but is also significantly converted into plastic deformation energy, which involves the irreversible energy dissipation of the material's internal dislocations, slip, and other microscopic mechanisms. At the same time, due to friction, microstructural rearrangement, and possible phase transitions during deformation, some of the input energy is also converted into thermal energy, resulting in a localized or overall increase in specimen temperature. These energy conversion processes together determine the stress–strain relationship, damage mode, and energy dissipation characteristics of the specimen during the test. In this paper, we will analyze the energy evolution characteristics under uniaxial compression with different pore morphologies in conjunction with the stage of stress–strain curves observed during the loading process. The evolution trend of energy under uniaxial action with the strain growth for the sandstone specimens with different pore section morphologies is shown in Figure 9.

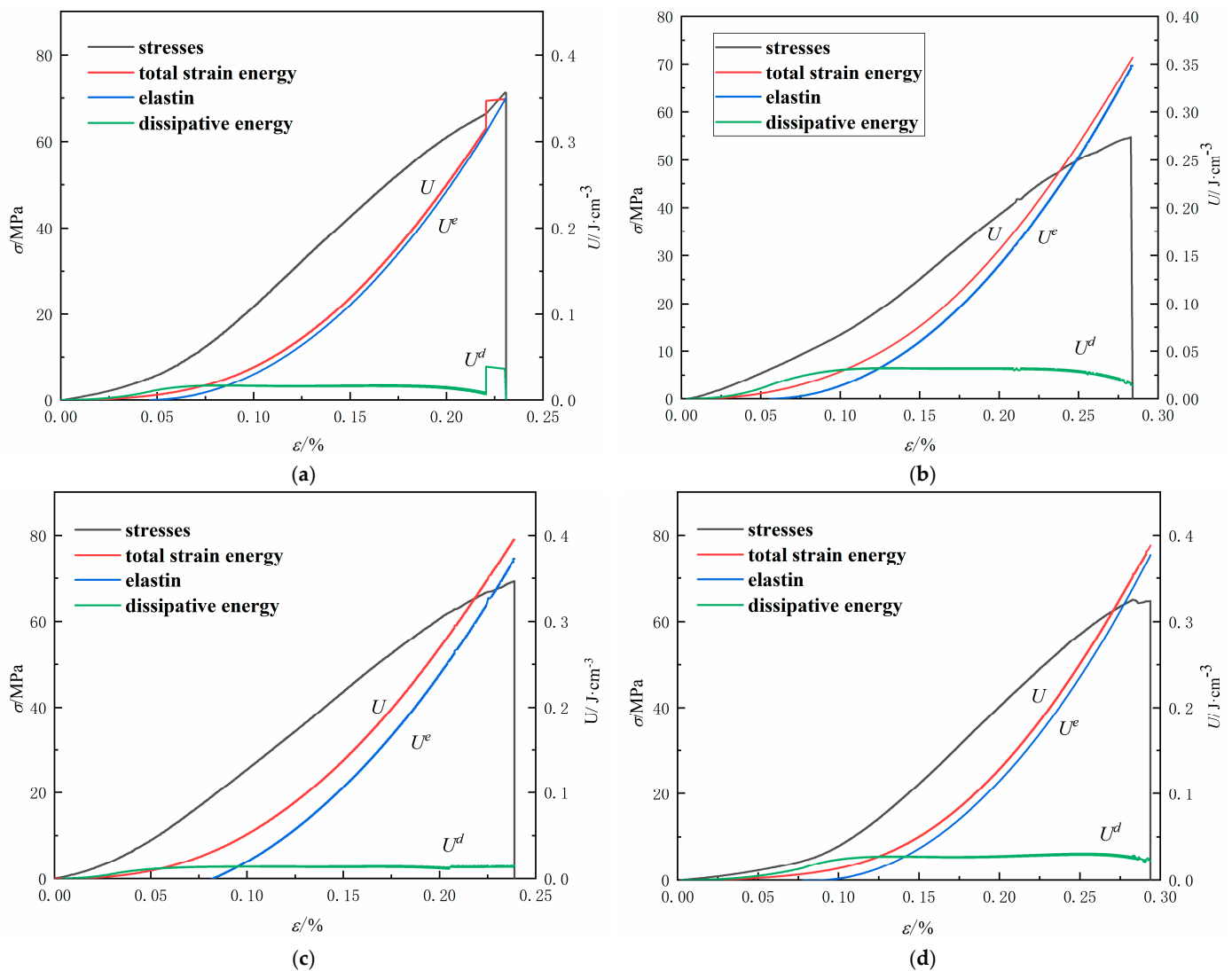


Figure 9. Trend of energy evolution of sandstone with different pore section forms. (a) Orbicular form; (b) Rectangular pattern; (c) Trapezoidal pattern; (d) Straight-wall domed form.

It is not difficult to see from the figure that the energy variation curves of sandstone with different pore section morphologies all exhibit a common characteristic, that is, the total strain energy and elastic energy increase in a concave curve, while the dissipated energy increases in a convex curve. This is because, in rock mechanics, when rock is subjected to external forces, it undergoes two stages, as follows: elastic deformation and plastic deformation, which correspond to different energy storage and dissipation modes. The manifestation of total strain energy, elastic energy, and dissipated energy during rock deformation is as follows: In the initial stage of external force application, the rock mainly undergoes elastic deformation, at which point the elastic energy increases rapidly, while the dissipated energy increases slowly. During this stage, the growth trends of the total strain energy and the elastic energy are similar, with both showing a rapid upward trend. The elastic deformation of rock is reversible, meaning that, when the external force is removed, the rock can return to its original state. As the external force continues to increase, the rock begins to transition from an elastic state to a plastic state. During this stage, the rate of increase in elastic energy gradually slows and reaches a peak before beginning to decrease. This signifies that the rock's elastic deformation capacity has reached its limit, and plastic deformation begins to occur. At the same time, the dissipated energy begins to increase significantly, indicating an intensification of energy dissipation caused by external forces. When the external force exceeds the rock's elastic limit, the rock enters the plastic deformation stage. During this stage, the elastic energy remains relatively constant or slightly decreases, while the dissipated energy continues to increase rapidly. The plastic deformation of rock is irreversible, meaning that, when the external force is removed, the rock cannot return to its original state. In summary, the increase in the elastic energy is fast at first, and then slows down, while the increase in dissipated energy gradually accelerates, leading to the concave curve of total strain energy and elastic energy and the convex curve of dissipated energy. This characteristic of the energy variation curve reflects the process of rock transitioning from an elastic response to a plastic response when subjected to external forces. The concave curve of total strain energy and elastic energy reflects a slowdown in the rate of increase in elastic energy during the transition from elastic deformation to plastic deformation, while the convex curve of dissipated energy reflects the accelerated accumulation of dissipated energy during plastic deformation. These curve morphologies are an intuitive representation of energy distribution and conversion characteristics that occur during axial compressive deformation of rock samples with pores.

It can be observed that the section specimens with straight-wall domed and trapezoidal holes accumulate more energy than the other two, both in terms of total strain energy and elastic energy, which is due to the special properties of the hole morphology. The presence of straight-wall domed and trapezoidal holes increases the perimeter of the rock specimens, and the complex morphology of the holes results in more stress concentration points and irregular stress distributions, relative to that of the circular and rectangular holes. Under uniaxial compressive loading, these morphologies of holes lead to more complex strain distributions and stress transfer paths, which increase the deformability and elastic deformation capacity of the rock specimens. As a result, the rock specimens are able to absorb and release more elastic energy when subjected to pressure, resulting in a significant increase in the value of the elastic energy curve. On the contrary, circular and rectangular holes, due to their more regular morphology and simpler stress distribution, have lower values of elastic and total energy curves compared to holes with complex morphology. This is because these hole patterns do not induce the same degree of stress concentration effect, and, therefore, they generally exhibit less elastic energy in compression tests.

Furthermore, their irregular morphology and boundary conditions often lead to more complex and tortuous crack extension paths within the specimen. These irregularly shaped holes guide crack expansion in different directions inside of the specimen, which results in more efficient and adequate energy dissipation during the loading process. In contrast, the crack extension paths of circular- and rectangular-hole specimens are relatively direct and simple, and the cracks are more likely to extend along the neutral axis or the

principal stress direction of the specimen, which may lead to less efficient energy absorption during uniaxial compression. In this case, the values of the total elastic energy curves of the specimens are relatively low, because the crack extension paths are relatively direct and the energy dissipation is not as adequate as that of the straight-wall domed and trapezoidal-hole specimens.

Therefore, the morphology and complexity of the holes directly affect the numerical performance of the elastic energy curves of the rock specimens in uniaxial compression tests, and the presence of straight-wall domed and trapezoidal holes leads to higher elastic energy output, which is macroscopically shown by the extremely active acoustic emission signals, and produces the occurrence of violent spalling, ejection, and fragmentation of the rock specimens.

6. Discussion

In this paper, the mechanical properties, damage modes, acoustic emission characteristics, and energy evolution laws of sandstones with different pore morphologies (circular, rectangular, trapezoidal, and straight-wall domed) under uniaxial compression are discussed. It was found that the pore morphology significantly affects the mechanical parameters of sandstone, and the damage modes and acoustic emission characteristics of sandstone with different pore morphologies are different. These research results can help to guide the optimization of coal mine roadway structures, improve the stability of the roadway, and prevent geologic roof disasters, which is of great significance to the safe production of coal. The limitation is that this thesis is established in the state of stress under uniform load, and, due to the complex spatial layout of shaft mining, this will also lead to uneven stress distribution at a certain period and to a certain extent, and the phenomenon of eccentric load occurs above the coal mine roadway, which induces different degrees of damage to the roadway section, etc. Therefore, the research can be continued for the development of this field.

7. Conclusions

Through uniaxial compression tests conducted on sandstone samples with various hole sections, along with an analysis of the stress–strain characteristic curves, fracture patterns, and acoustic emission event counts of different rock samples, an investigation was carried out to explore the characteristics, similarities, and differences in the microstructure of the fracture surfaces of sandstone samples with different hole sections. The brittle failure characteristics of sandstone under the experimental conditions were studied, and a preliminary analysis of the brittle failure mechanisms of sandstone with different hole sections was performed. Overall, the trapezoidal sections and the straight-wall circular-arch sections demonstrate superior stability and can withstand greater energy, making them the preferred choices for the design of underground roadway sections in coal mines. Their acoustic emission characteristic parameters and the gradual evolution of cracks can provide certain analytical tools for disaster early warning and forecasting. The specific conclusions are as follows:

- 1 The type of pore morphology is an important factor affecting the mechanical parameters of sandstone specimens. The generation of microfractures in the linear boundary pore specimen is greater, while the curved pore section morphology is the emergence of the tip raised transient brittle damage phenomenon, and its modulus of elasticity and peak stress have the same rise and fall of the characteristics of change.
- 2 The hole morphology shows that, in centrosymmetric hole types (circular holes and rectangular holes), more pressure-shear cracks and shear cracks appear, while, in axisymmetric hole types (trapezoidal holes and straight-wall arched holes), more tensile cracks and shear cracks appear.
- 3 The acoustic emission characteristics of holes with an axisymmetric shape (straight-wall domed and trapezoidal) show the characteristic properties of high-energy–high-amplitude–high-count of the “three highs.” On the other hand, the acoustic emission

characteristics of centrosymmetric holes (circular and rectangular) show the characteristic attribute of “two lows and one high” of “high-energy–low-amplitude–low-count,” and the stress change curve has good correspondence with the evolution trend of the acoustic emission ringing counts, and has nothing to do with the change in amplitude. The stress change curve has good correspondence with the evolution trend of the acoustic emission ring counts, but not with the amplitude change.

- 4 In the uniaxial compression test, the accumulation and dissipation of energy in the rock system are closely related to the morphology of the holes, and the trapezoidal and straight-wall domed holes are more conducive to the accumulation and release of energy, while the rectangular and circular holes have weaker energy accumulation and dissipation.

Author Contributions: G.L. and D.W. wrote the main text of the manuscript and the experimental data processing and summaries, while S.W., Y.Z., Q.Z., Z.Y., J.L. and Z.W. were the co-authors responsible for collecting the relevant information to organize the structure of the paper. All authors have read and agreed to the published version of the manuscript.

Funding: This research was funded by the Natural Science Foundation of Heilongjiang Province, grant number YQ2023E039; Basic Scientific Research Operating Expenses of Heilongjiang Provincial Universities and Colleges of China, grant number 2022-KYYWF-0554; the Scientific and Technological Key Project of “Revealing the List and Taking Command” in Heilongjiang Province, grant number 2021ZXJ02A03, 2021ZXJ02A04; Heilongjiang University of Science and Technology Introduces High-level Talents Scientific Research Start-up Fund Project, grant number HKD202304; Heilongjiang Provincial Undergraduate Colleges and Universities Basic Research Operating Expenses for Scientific Research Projects Young Talent Program Projects, grant number 2023-KYYWF-0513; the Gansu Provincial Youth Doctoral Support Program, grant number 2024QB-103; and the Gansu Youth Science and Technology Foundation, grant number 24JRRA1012.

Data Availability Statement: The datasets used and analyzed in this study can be provided by the authors Gang Liu and Dongwei Wang, according to reasonable requirements.

Acknowledgments: This research was supported by the Heilongjiang Ground Pressure and Gas Control in Deep Mining Key Laboratory, Heilongjiang University of Science and Technology.

Conflicts of Interest: The authors declare no conflicts of interest.

References

1. Meng, Q.; Han, L.; Qiao, W.; Lin, D.; Wei, L. Numerical simulation study on optimized design of section shape of deep high-stress soft rock roadway. *J. Min. Saf. Eng.* **2012**, *29*, 650–656.
2. Sun, G.; Chen, G.; Yu, P. Optimization design and application of deep mining roadway section. *Coal Eng.* **2008**, *9*, 57–60.
3. Dai, Y.; Chen, W.; Liu, Q.; Yi, X. Optimization of roadway section in deep high geostress. *J. Rock Mech. Eng.* **2004**, *S2*, 4960–4965.
4. Lv, A. Selection method of underground chamber section shape in high stress areas. *J. Coal Sci.* **1997**, *5*, 49–52.
5. Yang, S.; Xu, W.; Wei, L.; Su, C. Statistical ontological modeling and experimental study of rock damage under uniaxial compression. *J. Hohai Univ. (Nat. Sci. Ed.)* **2004**, *02*, 200–203.
6. Yang, S.; Lu, Z.; Qu, T. Fine-scale test and simulation of crack extension in marble with single pore. *J. China Univ. Min. Technol.* **2009**, *38*, 774–781.
7. Yang, S.; Liu, X.; Li, Y. Experimental analysis of mechanical properties of sandstone with pore-containing fractures under uniaxial compression. *J. Rock Mech. Eng.* **2012**, *31*, 3539–3546.
8. Liu, Z.; Li, Y. Experimental study on the deformation and rupture law of rocks with holes under uniaxial compression. *Eng. Mech.* **2010**, *27*, 133–139. [[CrossRef](#)]
9. Zhou, J.; Yang, K.; Fan, K.; Zhao, T.; Qiu, D. Influence of fracture on mechanical and damage evolution characteristics of pore-bearing sandstone. *J. Cent. South Univ. (Nat. Sci. Ed.)* **2019**, *50*, 968–975.
10. Li, G.; Zhang, N.; Wang, C.; Zhang, L.; Li, B. Numerical simulation study on optimization of section shape of high geostress roadway. *J. China Univ. Min. Technol.* **2010**, *39*, 652–658.
11. Du, M.; Jing, H.; Su, H.; Zhu, T. Effect of pore shape on strength and damage characteristics of sandstone. *Eng. Mech.* **2016**, *33*, 190–196+219.
12. Xu, L.; Guo, S.; Davide, E.; Liu, H.; Hong, Z.; Xiao, T. Zonal rupture pattern and control of surrounding rock structure in deep roadways with different sections. *J. Geotech. Eng.* **2023**, *45*, 720–729.

13. Gao, F. Numerical simulation analysis of the influence of section shape on the stability of roadway surrounding rock. *J. Shandong Univ. Sci. Technol. (Nat. Sci. Ed.)* **2007**, *02*, 43–46.
14. Liu, G.; Wang, D.; Yang, Z. Mechanical properties and acoustic emission characteristics of sandstone with three holes under bias load. *J. Heilongjiang Univ. Sci. Technol.* **2023**, *33*, 875–881.
15. Zhao, G.; Wang, E.; Wu, H.; Qiu, J.; Dai, Y. Fine-scale fracture evolution law of porous sandstone under uniaxial compression. *J. Cent. South Univ. (Nat. Sci. Ed.)* **2019**, *50*, 1891–1900.
16. Li, D.; Zhu, Q.; Li, X. Research on the effect of pore shape on the mechanical properties of marble progressive damage. *J. Undergr. Space Eng.* **2018**, *14*, 58–66.
17. Lu, S.; Ma, F.; Lu, Y. Numerical simulation analysis of the stability of roadway with different section shapes under impact load. *J. Saf. Environ.* **2017**, *17*, 76–80. [[CrossRef](#)]
18. Yao, Z.; Fang, Y.; Zhang, R.; Pu, S.; Zhao, G.; Yu, T.; Ma, C. The Mechanism of Stick–Slip as a Rockburst Source in Jointed Rockmass: An Experimental Study. *Rock Mech. Rock Eng.* **2023**, *56*, 3573–3593. [[CrossRef](#)]
19. Yu, T.; Fang, Y.; Yao, Z.; Pu, S.; Ye, L.; Zhao, G. Bearing effect of prestressed bolt-anchored structures and mechanical analysis of surrounding rock. *Chin. J. Geotech. Eng.* **2022**, *44*, 1069–1077.
20. Sun, Y.; Xu, S.; Xu, C.; Huang, W.; He, J.; Rong, Y.; Zheng, F.; Ding, L. Study on the Stress and Deformation of Surrounding Rock and Support Structure of Super Large Section Tunnels Based on Different Excavation Methods. *Appl. Sci.* **2024**, *14*, 7025. [[CrossRef](#)]
21. Xu, H.; Zhang, Z.; Zhang, Y.; Jiang, Q.; Qiu, S.; Zhou, Y.; Feng, G. Effects of natural stiff discontinuities on the deformation and failure mechanisms of deep hard rock under true triaxial conditions. *Eng. Fail. Anal.* **2024**, *158*, 108034. [[CrossRef](#)]
22. Gu, H.; Lai, X.; Tao, M.; Momeni, A.; Zhang, Q. Dynamic mechanical mechanism and optimization approach of roadway surrounding coal water infusion for dynamic disaster prevention. *Measurement* **2023**, *223*, 113639. [[CrossRef](#)]
23. Zhu, T.; Jing, H.; Su, H.; Su, H.; Yin, Q.; Du, M. Experimental study on uniaxial compressive mechanical properties of sandstone containing double circular holes. *J. Geotech. Eng.* **2015**, *37*, 1047–1056.
24. Liu, G.; Wang, D.; Zan, Y.; Wang, S.; Zhang, Q. Feasibility Study of Material Deformation and Similarity of Spatial Characteristics of Standard Coal Rocks. *Processes* **2024**, *12*, 454. [[CrossRef](#)]
25. Song, Y.; Xing, T.; Zhao, T.; Gao, P. Acoustic emission characterization of uniaxial compressive deformation field evolution in rocks. *J. Rock Mech. Eng.* **2017**, *36*, 534–542. [[CrossRef](#)]
26. Xu, S.; Tong, L.H.; Xu, C.; Ding, H. On wave transmission in saturated soil system separated by a nonlinear isolated layer. *Comput. Geotech.* **2021**, *136*, 104211. [[CrossRef](#)]
27. Feng, G.; Ma, Q.; He, Z.; Su, G.; Chen, B. Time-delayed failure process of granite and its energy evolution and acoustic emission characteristics. *Eng. Fail. Anal.* **2024**, *157*, 107854. [[CrossRef](#)]
28. Zhang, Z. Energy Evolution Mechanism During Rock Deformation and Destruction. Ph.D. Thesis, China University of Mining and Technology, Beijing, China, 2013.
29. Zhang, Z.; Gao, F. Experimental study on energy evolution of red sandstone under uniaxial compression. *J. Rock Mech. Eng.* **2012**, *31*, 953–962.
30. Xie, H.; Peng, R.; Ju, Y. Analysis of energy dissipation during rock deformation and damage. *J. Rock Mech. Eng.* **2004**, *21*, 3565–3570.
31. Xie, H.; Ju, Y.; Lai, L. Rock strength and overall damage criterion based on the principle of energy dissipation and release. *J. Rock Mech. Eng.* **2005**, *17*, 3003–3010.
32. Zhang, G.; Zhao, Y.; Sun, Y.; Gong, Z. Study on energy evolution and infrared radiation characteristics of different seam coals under uniaxial compression. *Coal Sci. Technol.* **2024**, *11*, 1–13.
33. You, M.; Hua, A. Energy analysis of the damage process of rock specimens. *J. Rock Mech. Eng.* **2002**, *06*, 778–781.
34. Liang, C.; Li, X.; Wang, S.; Li, S.; He, J.; Ma, C. Experimental study on rate correlation and energy mechanism of uniaxial compressive stress-strain characteristics of rocks. *J. Rock Mech. Eng.* **2012**, *31*, 1830–1838.
35. Hou, Z.; Wang, Y.; Liu, D.; Li, C. Study on mechanical properties and energy evolution anisotropy of laminated marble rupture process. *J. Min. Saf. Eng.* **2019**, *36*, 794–804. [[CrossRef](#)]
36. Liu, G. Mechanical Response Mechanism and Engineering Application of Sandstone Under Unloading Path. Ph.D. Thesis, Anhui University of Technology, Huainan, China, 2021. [[CrossRef](#)]
37. Liu, G.; Xiao, F.; Qin, T. Mechanical properties and acoustic emission law of rock under small size effect. *J. Rock Mech. Eng.* **2018**, *37*, 3905–3917. [[CrossRef](#)]

Disclaimer/Publisher’s Note: The statements, opinions and data contained in all publications are solely those of the individual author(s) and contributor(s) and not of MDPI and/or the editor(s). MDPI and/or the editor(s) disclaim responsibility for any injury to people or property resulting from any ideas, methods, instructions or products referred to in the content.